AIAA 81-1214R

Aerodynamic Features of Designed Strake-Wing Configurations

John E. Lamar* and Neal T. Frink†
NASA Langley Research Center, Hampton, Va.

Sixteen analytically and empirically designed strakes have been aerodynamically tested on a common wing-body to determine the longitudinal characteristics of the configurations. These strakes were selected, in general, owing to their superior performance in a water-tunnel test. There they exhibited a good correlation between the hypothesized high value of angle of attack for strake-vortex breakdown and the high value of leading-edge suction at the strake tip. The lift and pitch data were reasonably well predicted by an extended suction analogy method, and the lift agreement improved with increasing strake area. The strake-vortex-breakdown angle and configuration maximum lift generally increase with increasing strake area and, to some extent, strake tip leading-edge suction value. The best strake configurations all developed about the same maximum area efficiency despite their differences in size.

Nomenclature

AD	= analytically designed
b	= span, wing span = 50.8 cm (20 in.)
$C_{D,0}$	= zero-lift drag coefficient = drag/$q_\infty S_{ref}$
C_L	= lift coefficient = lift/$q_\infty S_{ref}$
$C_{L,max}$	= maximum value of $C_{L,tot}$
C_m	= pitching moment coefficient about the 56.99% body length station = (pitching moment)/$q_\infty S_{ref} c_{ref}$
c_{ref}	= reference chord = 23.33 cm (9.185 in.)
ED	= empirically designed
f	= additional lifting surface efficiency factor = $(C_{L,tot})_{swb}/(C_{L,tot})_{wb}\ [1/(1+R_a)]$
LE	= leading edge
M	= freestream Mach number
q_∞	= freestream dynamic pressure
R_a	= ratio of exposed strake area to wing reference area = S_s/S_{ref}
R_b	= exposed semispan ratio = $[(b/2)_s/(b/2)_w]_{exp}$
R_N	= Reynolds number
S	= area
S_{eff}	= effective area; exposed strake area and the wing area enclosed between the root and the tip of the exposed strake
S_{ref}	= reference wing area = 0.1032 m^2 (1.1109 ft^2)
s	= (section suction force)/$[q_\infty \alpha^2 (b/2)]$
TE	= trailing edge
α	= angle of attack, deg
$\alpha_{BD\text{-}TE}$	= angle of attack at which strake vortex breaks down at wing trailing edge, as determined from total lift data characteristics, deg
α_{eq}	= angle of attack at which total lift data equal the high-α theory value, deg
η_s	= fraction of exposed strake semispan
Λ	= wing leading-edge sweep, deg

Subscripts

exp	= exposed
s	= strake
swb	= strake-wing-body configuration
t	= tip
tot	= total for the strake-wing-body configuration unless otherwise denoted
w	= wing
wb	= wing-body configuration
$\alpha_{BD\text{-}TE}$	= evaluated at $\alpha_{BD\text{-}TE}$

Introduction

STRAKE-WING configurations are becoming of increasing interest for maneuvering aircraft owing to the mutual benefits derived from this geometric combination (see Refs. 1-3). These benefits include for the wing: 1) minimal interference at or below the cruise‡ angle of attack, 2) energizing of upper surface boundary layer with the resulting flow reattachment on the outer wing panel at moderate to high angle of attack due to the strake vortex, and 3) reduced area required for maneuver lift. Benefits for the strake are 1) upwash from the main wing strengthens strake vortex and 2) the need for only a small area (hence wetted area and comparatively lightweight structure) to generate its significant contribution to the total lift, because the strake provides large amounts of vortex lift. It should be mentioned that these vortex-induced benefits are realized when the strake vortex is stable and maintaining a well-organized vortex system over the wing. Once the angle of attack becomes sufficiently large that strake-vortex breakdown progresses ahead of the wing trailing edge, these favorable effects deteriorate significantly.

In view of the aforementioned importance of the vortex stability it is appropriate to consider how best to maintain it by proper shaping of the strake. A method was developed and implemented in Ref. 4 for determining strake shape based on a theoretical leading-edge suction distribution. The main idea was that those distributions which tended to peak toward the tip were hypothesized to be the better ones and lead to improved strake shapes. After this initial design effort others were designed, tested by the authors in the Northrop Diagnostic Water Tunnel in a cooperative program, and reported on in Refs. 5 and 6. The strakes tested included 24 analytically designed ones and 19 empirically designed ones, with each set mounted on the same wing-body model. The

Presented as Paper 81-1214 at the AIAA 14th Fluid and Plasma Dynamics Conference, Palo Alto, Calif., June 23-25, 1981; submitted July 13, 1981; revision received Nov. 12, 1981.

*Aeronautical Research Scientist, Fluid Dynamics Branch, Subsonic-Transonic Aerodynamics Division. Associate Fellow AIAA.

†Aero-Space Technologist, Fluid Dynamics Branch, Subsonic-Transonic Aerodynamics Division. Member AIAA.

‡In particular, at cruise it is possible that the small impact of the strake may only be attainable by the use of camber or dihedral so as to "unload" the strake under this condition. Neither one of these is addressed in this paper, as only planar strakes are considered.

analysis in the preceding references showed that the angle of attack at which the strake vortex began to break down at the wing trailing edge correlated well with the strake tip value of the theoretical, three-dimensional, potential-flow, leading-edge suction. This correlation then tends to confirm the supposition that the strake leading-edge suction is a critical parameter and one which may be useful in strake design or assessment.

From these water-tunnel tests, 16 strake-wing-body configurations, seven analytically designed and nine empirically designed, were considered of sufficient interest to be tested on a similar wing-body model in a wind tunnel to obtain force data and to extend the Reynolds number range. These tests, like those in water, were to be performed at zero sideslip because of the large test matrix involved.

The purpose of this paper is to summarize the effects of the various geometric parameters and to evaluate to what extent these tip suction values are related to the measured vortex lift characteristics.

Model Description

General

A drawing of a typical configuration is shown in Fig. 1. It should be noted that the model features forebody and afterbody components separated by a metric break for multiple component aerodynamic testing. Total loads were measured by the main balance located in the aft fuselage while strake-forebody loads were measured by the forebody balance attached to but ahead of the metric break. The models were tested in the Langley 7×10-ft High-Speed Tunnel and standard corrections were applied to the measured data to obtain the results presented. It should be noted that the wing and strakes are thin, not warped and have sharp leading edges.

Strakes

The various strakes tested on this wing-body are divided into the two groups of analytically designed (AD) and empirically designed (ED), as shown in Figs. 2 and 3, respectively, and are ordered on each figure according to the value of leading-edge suction at the strake tip s_t. (The strake tip is defined as the intersection of the strake and wing panel leading edges.) A complete description of these strakes is given in Ref. 7; therefore only a brief overview of the strake geometries are included herein (see Table 1).

For the AD strakes all are gothic in planview except for the AD 9, which is reflexive. For the ED group, which is derived from the AD 24 by a series of systematic cuts and chord scalings, all are gothic or gothiclike. Some are generated by cutting parallel to the apex at increasing values of η_s along the leading edge, ED 2 and ED 4; others by cutting parallel to the trailing edge at decreasing values of η_s along the leading edge, ED 5 and ED 6; others by cutting parallel to and along the inboard edge to leave 0.85 $(b/2)_{s,exp}$, 0.70 $(b/2)_{s,exp}$, and 0.55 $(b/2)_{s,exp}$ amount of the original strake semispan remaining for the ED 9, ED 10, and ED 11, respectively; and lastly, two are obtained by scaling (reducing) the chord at each span station to 70 and 30% of the AD 24 chord value to yield the ED 12 and ED 13, respectively.

It should be noted that in this paper the complete configuration of strake-wing-body is denoted by the strake designation.

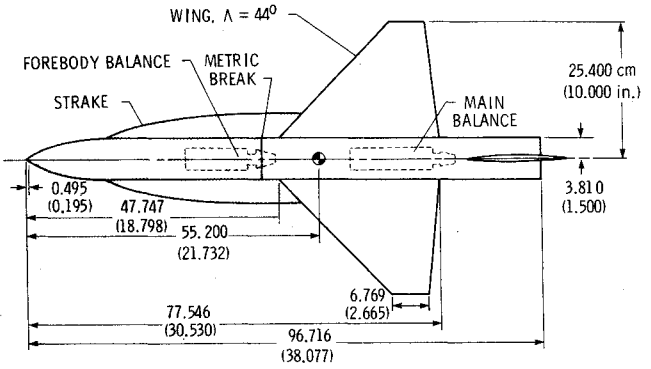

Fig. 1 Planform sketch of general configuration.

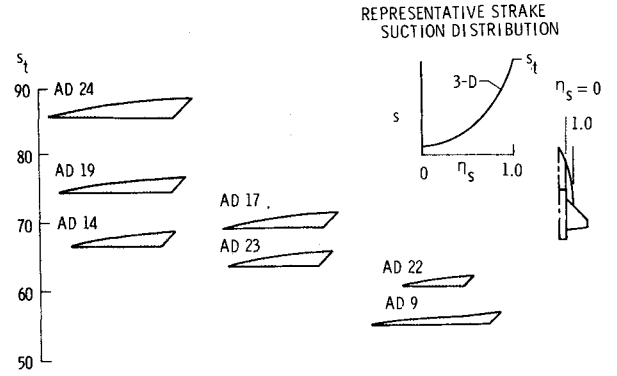

Fig. 2 Analytically designed (AD) strakes selected from water-tunnel test.

Table 1 Strake/configuration geometric and aerodynamic features

Configuration designation	R_a	R_b	R_s	S_{eff}/S_{ref}	s_t	α_{eq}, deg	$\alpha_{BD\text{-}TE}$, deg	C_L, max	f Fig. 15	f_{max}	$\partial f/\partial R_a C_{L,max}$
AD 9	0.183	0.197	10.65	0.397	56.9	18.45	27.6	1.54	...	1.50	...
AD 14	0.172	0.212	6.99	0.415	66.7	14.22	28.5	1.63	1.62	1.62	3.58
AD 17	0.185	0.212	7.77	0.428	69.3	14.82	29.4	1.69	1.63	1.63	3.42
AD 19	0.205	0.212	8.50	0.448	73.4	16.09	30.4	1.76	1.62	1.64	3.25
AD 22	0.077	0.144	7.00	0.247	61.1	14.30	17.4	1.23	1.19	1.30	2.25
AD 23	0.166	0.212	7.00	0.409	64.0	14.61	28.2	1.59	1.42	1.54	2.34
AD 24	0.325	0.297	7.00	0.653	86.5	24.59	31.0	1.99	1.63	1.65	1.23
ED 2	0.266	0.297	5.19	0.594	90.2	...	31.6	1.88	1.54	1.59	1.66
ED 4	0.114	0.297	2.77	0.442	31.1	7.10	25.0	1.37	1.35	1.42	2.25
ED 5	0.188	0.262	5.83	0.482	69.8	18.52	29.2	1.72	1.65	1.66	3.39
ED 6	0.124	0.226	5.22	0.381	42.3	15.96	23.8	1.40	1.34	1.41	1.64
ED 9	0.259	0.253	7.79	0.543	96.0	22.35	31.5	1.88	1.64	1.64	1.76
ED 10	0.192	0.208	8.62	0.430	103.1	19.86	29.6	1.69	1.60	1.61	3.43
ED 11	0.131	0.163	9.59	0.322	117.2	17.49	23.6	1.38	1.27	1.39	2.10
ED 12	0.227	0.297	5.18	0.555	65.5	18.89	30.5	1.78	1.55	1.59	1.33
ED 13	0.098	0.297	2.78	0.426	40.5	...	20.8	1.32	1.26	1.37	2.65

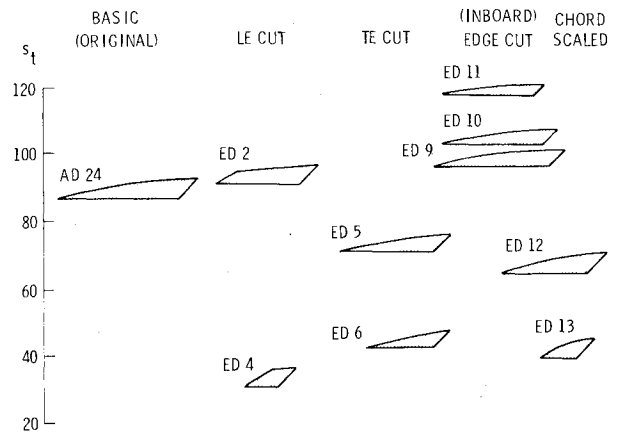

Fig. 3 Empirically designed (ED) stakes selected from water-tunnel test.

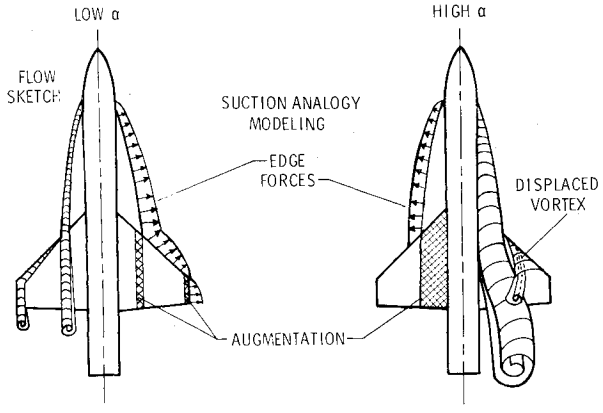

Fig. 4 Theoretical vortex lift model for strake wing.

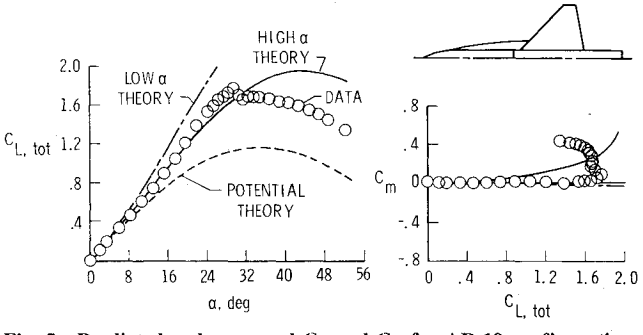

Fig. 5 Predicted and measured C_L and C_m for AD 19 configuration; $M=0.2$.

Theoretical Modeling for Analysis

A method for estimating the aerodynamic forces and moments for strake-wing-body configurations having leading- and side-edge vortex flows is documented in Ref. 8. This method estimates the vortex flow effects with the suction analogy and the basic potential flow effects with the vortex lattice method of Ref. 9. In addition, the effect of the forward shed vorticity acting over a downstream surface, such as strake vortex on the wing, has been quantified and is identified as an augmented vortex flow term .[7] These pieces are put together in two different ways depending upon the applicable angle-of-attack range, as can be seen from Fig. 4, and justified below.

From oil flow photographs at low angle of α, it was concluded that the configuration had attached flow away from the leading and side edges, and downstream from the component tips, vortical flow existed. However, at the higher values of α, the strake vortex becomes much larger and tends

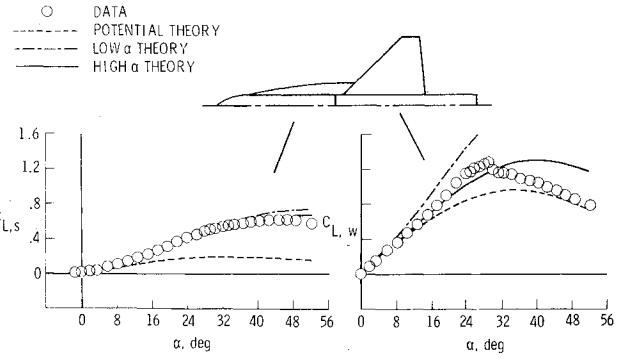

Fig. 6 Predicted and measured component C_L for AD 19 configuration; $M=0.2$.

to displace the wing-vortex-flow system off the wing, so that this system can no longer cause flow reattachment to occur on the wing. This lack of reattachment causes a large portion of theoretically available aerodynamic effects to be effectively lost to the configuration. These two solutions are called the low-α and the high-α vortex lift theories, or, in shortened form, low-α and high-α theories.

These two theoretical solutions along with the potential-flow one are used subsequently in comparison with the data.

Data Results and Discussion

Predicted and Measured Results

Data have been obtained on these 16 configurations at values of α up to ≈ 50 deg for the subcritical Mach number values of 0.2, 0.5, and 0.7. Only the $M=0.2$ data will be analyzed herein, as the other data, presented in Ref. 7, generally yield similar conclusions.

Typical Results

Typical of the total configuration lift and pitching moment results are those for the AD 19 configuration given in Fig. 5. The drag data are not given since their variation is just $C_{D,0}+C_L \tan\alpha$ for these thin unwarped lifting surfaces. From Ref. 7 it was determined that in general for this and the other configurations, the C_L data are better estimated by the high-α theory. Though better estimated, there may be an α range below the α for $C_{L,max}$ for which the C_L data are underpredicted. This is most likely associated with the exclusion in the high-α theory of any vortex lift from the wing. A further reflection of this exclusion is seen in the C_m vs C_L results, where the theory shows the center of pressure to be ahead of the data. The potential-flow curve is added to the $C_{L,tot}$ vs α plot for reference in Fig. 5.

Component data for the strake-forebody and wing-afterbody were also obtained from the wind-tunnel tests and are reported in Ref. 7. Typical lift data and theoretical estimates are shown in Fig. 6 for the AD 19 configuration. The outcome is the same as given in Ref. 8, where the individual C_L data are generally well estimated by the high-α theory or a combination of the high-α and low-α theories. The component C_m results are tightly bracketed by the high-α and low-α theories up to the individual values of $C_{L,max}$, or the occurrence of large-scale vortex breakdown.

Since the $C_{L,tot}$ vs α variation is reflective of the strake vortex performance, only this aerodynamic characteristic will be employed in subsequent data analysis.

Lift Ratios

One convenient way to summarize the C_L data for the total configuration is to present them normalized by the high-α theory, $C_{L,tot}$ theory, results. This is done for the AD 19 configuration and presented in Fig. 7 along with lift ratio variations for two other analytically designed strake configurations, the AD 17 and the AD 24.

Unmodeled Flow Features: These curves show that the theory predicts the data to within ±10% for values of $\alpha \leq 36$ deg. In particular, all three curves demonstrate an initial theoretical overestimation of the data by ≈5% followed by an underestimation ≥10%. The overestimation is slight, indicating the flow to be modeled well in that α range, whereas at slightly higher values of α, the underestimation (generally a larger percentage value) is indicative of the unmodeled flow features becoming important. These stem primarily from the neglected effects of the wing leading-edge vortex system. This latter range of α is followed by another in which these same three curves become progressively less than 1.0 with increasing α. This behavior is indicative that strake-vortex breakdown has occurred in the test data, but not (since it is not modeled or accounted for) in the high-α theory.

Figure 8 presents the $C_{L,\text{tot}}$ ratio curves for the remaining analytically designed strakes and for four of the better empirically designed strakes. All but one of these curves has a similar variation to those curves presented in Fig. 7.

α_{eq}: Figure 7 is also used to define α_{eq}, so named because it is the smallest α value which is ≥12 deg where the $C_{L,\text{tot}}$ ratio curve *equals* a value of 1.0. These crossings are denoted on this figure for all three configurations, and are summarized on Fig. 9 with those of the other 13 configurations which satisfy the α_{eq} definition. They are presented in this figure in terms of pertinent geometrical parameters.

From Fig. 9 it is clear with increasing values of R_a that α_{eq} will increase regardless of the R_b value. This means that one could expect to estimate better the $C_{L,\text{tot}}$ data to a higher value of α with increased strake area. This expectation is more likely associated with the more dominant effect a large strake plays on the configuration in terms of the resulting flowfield, and the corresponding better modeling representation which occurs at the higher values of α.

The α_{eq} data do not behave in a well-defined manner with R_b at a fixed value of R_a. Hence the only geometric parameter with which α_{eq} is correlated is R_a.

Analysis of Data

Additional correlations between aspects of the lift-dependent data and the geometric parameters can be determined by a process of data analysis which is given in the following paragraphs.

Correlations of $\alpha_{\text{BD-TE}}$

Correlations of the angle of attack at which strake-vortex breakdown crosses the wing trailing edge, $\alpha_{\text{BD-TE}}$, with the Reynolds number, strake geometry parameters, and aerodynamic or design features are discussed in this section. In particular, mathematical correlations between the preceding are sought.

Reynolds Number Effects: Since the $\alpha_{\text{BD-TE}}$ data from the water tunnel were instrumental in the selection of the 16 strakes tested in the wind tunnel, it was considered useful to investigate the Reynolds number effects brought about by testing in these two different fluids. Figure 10 shows that there is a significant difference in $\alpha_{\text{BD-TE}}$ for identical strake configurations, where both sets of data have been corrected for wall effects. The differences noted between the water and wind-tunnel results are most likely associated with the two-order-of-magnitude difference in Reynolds number. This can influence the configuration boundary layer and pressure field characteristics, as well as the characteristics of the strake core itself.[10] However, the similarity in the $\alpha_{\text{BD-TE}}$ trend with R_a at a fixed value of R_b§ for water and air show that the water

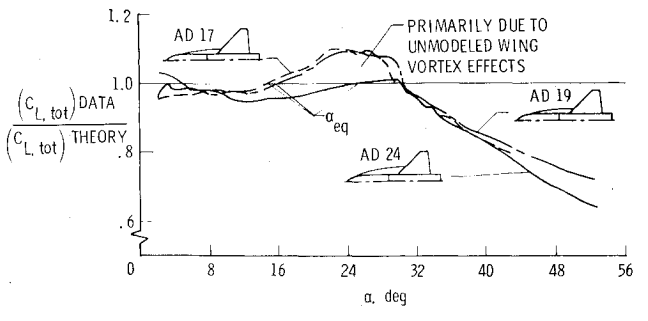

Fig. 7 Effect of α on theoretical modeling accuracy of $C_{L,\text{tot}}$; $M = 0.2$.

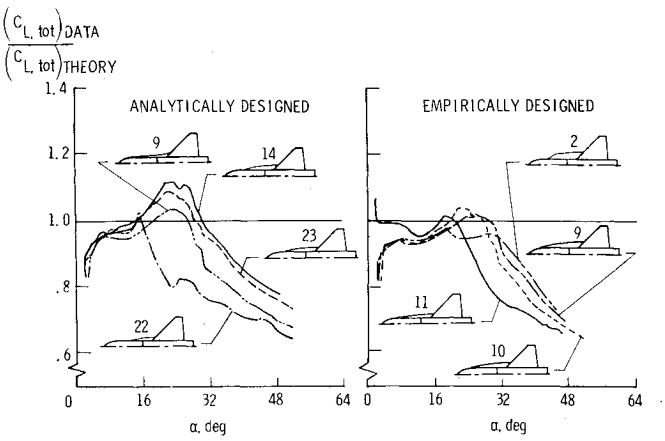

Fig. 8 Effect of α on theoretical modeling accuracy of $C_{L,\text{tot}}$ for other strakes; $M = 0.2$.

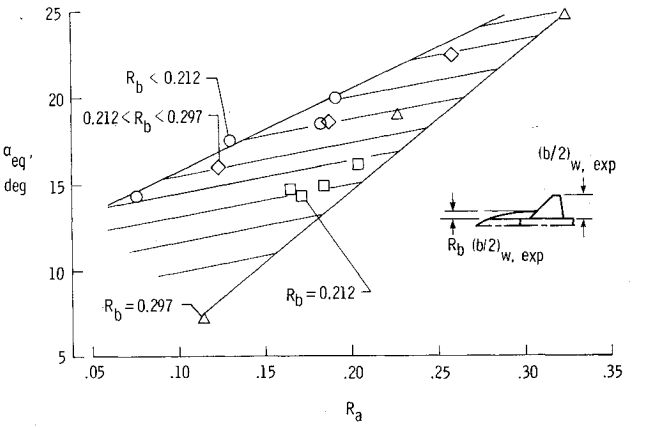

Fig. 9 Effect of span ratio on α_{eq}; $M = 0.2$.

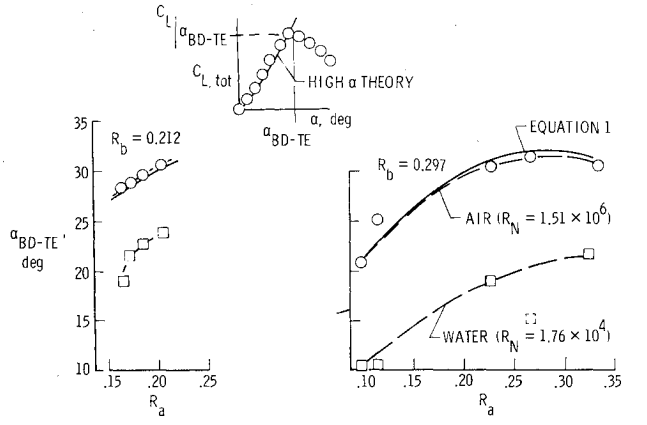

Fig. 10 Effect of Reynolds number on strake-vortex $\alpha_{\text{BD-TE}}$; $M = 0.2$.

§Note the dashed symbol for the $R_b = 0.297$ and $R_a = 0.260$ water-tunnel results. It represents an anomalous, though repeatable, data point.

tunnel can be a valuable qualitative research tool even with this large Reynolds number difference.

It is interesting to note in Fig. 10 that $\alpha_{BD\text{-}TE}$ in air is defined, using an inset, as the angle of attack at which there is a sudden decrease in the rate at which lift is being generated; this, for many cases, occurred just after $C_{L,max}$. Furthermore, this definition was verified for two configurations by natural flow visualization observed during the wind-tunnel test as the α for which strake-vortex breakdown occurred ahead of the wing trailing edge. These two configurations were the AD 24 and ED 5, and the associated values of $\alpha_{BD\text{-}TE}$ were 30 deg→32.5 deg and 28 deg, respectively, from flow visualization. These results, when compared with those in Table 1, help establish an accuracy of the tabulated number of $\approx \pm 1$ deg. The $\alpha_{BD\text{-}TE}$ values for the wing-afterbody component are $\simeq 1$ deg smaller than those tabulated for the complete configuration. This substantiates that a proper, systematic interpretation of the $C_{L,tot}$ data has been made.

While at least a qualitative correlation of $\alpha_{BD\text{-}TE}$ has been established between the two fluids, a way is sought by which to quantify the variation of $\alpha_{BD\text{-}TE}$ with R_a in air. This is pursued next.

Area Ratio: The dependence of $\alpha_{BD\text{-}TE}$ on R_a for the seven configurations shown in Fig. 10, and for the other nine configurations whose data are tabulated in Table 1 but not shown, appears to be a smooth one. Hence a curve fit was attempted using the data for the 16 strakes. The resulting relationship is that

$$\alpha_{BD\text{-}TE} = 32\sqrt{\sin[2\pi(R_a - 0.03)]} \text{ deg} \qquad (1)$$

The quality of this fit is good and can be seen for the strakes presented on Fig. 10 by the solid curve. Hence preliminary estimates of $\alpha_{BD\text{-}TE}$ can be made prior to wind-tunnel testing for other gothiclike strakes on this wing-body combination by only knowing R_a. However, since there are R_b effects on the data at low R_N, there may also be an impact of R_b and R_N on the estimation of $\alpha_{BD\text{-}TE}$ for $R_N > 1.51 \times 10^6$.

There still is an important relationship which needs to be established, and it is between $\alpha_{BD\text{-}TE}$ and the aerodynamic design parameter s_t.

Tip Suction Parameter: From the water-tunnel data presented in Ref. 6, it was shown that the tip value of the potential-flow, leading-edge suction parameter, s_t, generally increases as $\alpha_{BD\text{-}TE}$ increases. Immediately one can conclude that owing to the previously noted similarity of trend of $\alpha_{BD\text{-}TE}$ with R_a in air and water, a similar variation of s_t with $\alpha_{BD\text{-}TE}$ in air is expected and the data in Table 1 support this conclusion. However, s_t is not as strong a correlating parameter as R_a.

Associated with $\alpha_{BD\text{-}TE}$ is a value of $C_{L,tot}$ which is denoted by $C_{L,tot}|_{\alpha_{BD\text{-}TE}}$, defined in Fig. 10, and frequently equal to $C_{L,max}$. It is therefore useful to consider if $C_{L,max}$ correlates with one or more geometrical parameters.

Correlation of $C_{L,max}$

Since $C_{L,max}$ can be expected to increase with strake area, these data for the gothiclike strake configurations are graphed as a function of R_a in Fig. 11. It is seen that for all analytically and empirically designed strakes, a single curve can be used to correlate the $C_{L,max}$ increase with R_a. Though there is some small data scatter about this faired curve, R_a is, as expected, a good correlating parameter. There is one obvious feature of this curve and it is the marked decrease in the gradient of $C_{L,max}$ at $R_a \approx 0.20$. The reason for the sudden increase in $\partial C_{L,max}/\partial R_a$ is not clear and should be the subject of further study.

This figure also shows the aerodynamic parameter s_t to provide a lower bound value (note the exception) that separates strake configurations into those which generate smaller and larger values of $C_{L,max}$. The value of s_t which forms the bound is 64. A refinement of this general bound can be made by examining in Fig. 12 the $C_{L,max}$ and R_a data as a function of s_t. This figure shows that both of these quantities peak at $s_t = 86.5$ and, moreover, have their larger values in the range of $\sim 70 \le s_t \le 100$. Hence an aircraft designer would probably seek strake-wing configurations which produce s_t values in this range in order that the strakes be considered efficient lift producers. (Strake efficiency, in terms of area, is discussed in more detail subsequently.)

Figure 11 also shows a reference curve of $(C_{L,max})_{wb}(1 + R_a)$ which is used for comparison. Taking these two curves together is another way of seeing that addition of area in the form of a strake is a more efficient producer of $C_{L,max}$ than just enlarging the wing while keeping the reference area constant.

It was demonstrated in Ref. 2 that the strake incremental C_L data could be nearly collapsed when multiplied by S_{ref}/S_{eff}. The significance of this parameter is that it nondimensionalizes S_{ref} with respect to an "effective" area which incorporates the strake area and the wing area enclosed between the root and the tip of the exposed strake. The physical meaning of using this area is fairly clear for the strake lift increment, while for $C_{L,max}$ the reciprocal of this ratio has been determined to be useful, even though its physical meaning is not as clear. Nonetheless, the result was noteworthy in that the data for the gothiclike strake configurations could be correlated with the relationship

$$C_{L,max} = (1.53/R_b^{0.6})S_{eff}/S_{ref} \qquad (2)$$

Though this equation is for the strake-wing-body configurations discussed herein, it may be useful for others as well.

The generation of a large value of $C_{L,max}$ is important for strake-wing configurations, but generating it efficiently is also important in terms of using the strake area available in the most efficient way. This is taken up next, where not just $C_{L,max}$ but the entire $C_{L,tot}$ variation with α is considered.

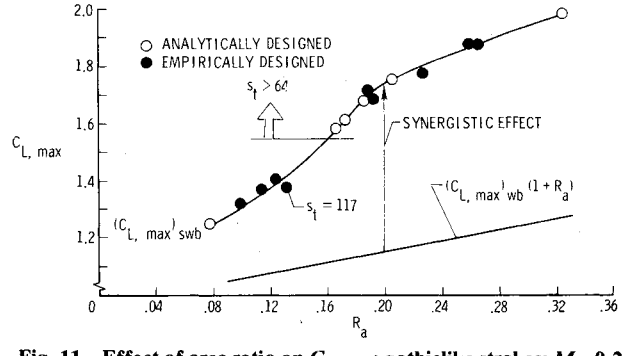

Fig. 11 Effect of area ratio on $C_{L,max}$: gothiclike strakes; $M = 0.2$.

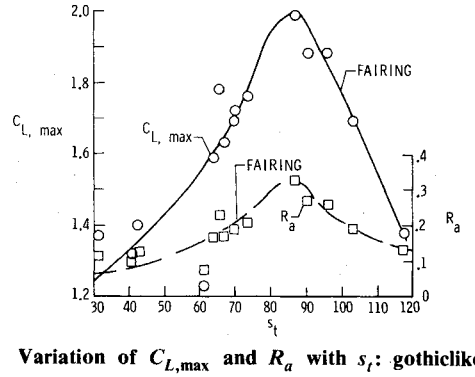

Fig. 12 Variation of $C_{L,max}$ and R_a with s_t: gothiclike strakes; $M = 0.2$.

Strake Efficiency

One way to assess strake efficiency with regard to maneuver capability is to compare the increase in lift obtained with the strake in place with what would have been expected by enlarging the wing area by an equal amount.

In equation form, this can be expressed by the parameter f:

$$f \equiv \frac{(C_{L,\text{tot}})_{\text{swb}}}{(C_{L,\text{tot}})_{\text{wb}}}\left(\frac{S_{\text{ref}}}{S_{\text{ref}}+S_s}\right) = \frac{(C_{L,\text{tot}})_{\text{swb}}}{(C_{L,\text{tot}})_{\text{wb}}(1+R_a)} \equiv \frac{\text{Total } C_L \text{ including aerodynamic synergism}}{\text{Scaled wing-body } C_L \text{ with increased area}} \quad (3)$$

which is given the name "additional lifting surface efficiency factor" in Ref. 8. The condition of $f>1$ will exist when the incremented increase in C_L associated with adding the area in the form of a strake exceeds the direct effect of that produced by increasing the basic wing area. The satisfaction of this condition means that, from a lift production standpoint, adding strake area is more efficient than just increasing wing area.

Theoretical Estimate

Figure 13 shows the experimental and theoretical variation of f with α for a representative configuration (AD 19). The theoretical curve for f uses the high-α vortex lift theory for the strake-wing-body configuration (numerator) and potential theory for basic wing-body (denominator) since each best approximates its respective data. Figure 13 shows that above $\alpha \simeq 14$ deg the theoretical and experimental values of f exceed unity because of the synergistic vortex lift being generated on the configuration. This figure also shows that for 17 deg $\leq \alpha \leq$ 40 deg the experimental results produce values of f greater than predicted by the theory. The increase in f is the result of a reduction in measured $(C_{L,\text{tot}})_{\text{wb}}$ which is due primarily to the loss of lift effectiveness on the basic wing associated with its own leading-edge vortex breakdown and large-scale stall. [The remainder of the difference, ~25%, is due to the high-α theory underpredicting the $C_{L,\text{tot}}$.] If the usual leading-edge flow control devices were applied to the wing, the flow would be more potential-like and the difference between the two f curves would be expected to diminish considerably. As a further note, it can be seen by comparing Fig. 13 with Fig. 5 that the maximum or peak value of f occurs at the same angle of attack as the maximum $(C_{L,\text{tot}})_{\text{swb}}$. This has been determined to be generally true. The second peak in f vs α, which occurs at $\alpha \approx 44$ deg, results from a sudden poststall loss of measurable lift on the wing-body, $(C_{L,\text{tot}})_{\text{wb}}$.

Most Efficient Strakes

In Fig. 14, the f vs α curves are presented for the AD 14, AD 17, AD 19, and AD 24 configurations, which, from a variety of considerations, appear to be among the most efficient ones tested. The figure shows the values for $f_{\max}$ for all four to be comparable, though the value of $f_{\max}$ for the AD 24 configuration is slightly higher. This comparison is particularly significant since the AD 14, AD 17, and AD 19 strakes have areas which range from 53-63% of the AD 24 strake and still produce these high values of $f_{\max}$. What is of even more significance is that the relative ordering of efficiences for the strakes follow the same relative ordering of s_t in Fig. 2; the higher s_t associated with the more efficient strake. Hence this tends to confirm the hypothesis that s_t may be a useful parameter in aerodynamic strake design.

Other Performance Considerations

In this section further studies are reported on with regard to f. In particular from the preceding discussions of the f variation with α for some of the most efficient strakes, it is clear that f has an R_a dependence. Though it is slight for the presented strakes in the α range for f up to $f_{\max}$, the behavior should be explored in further assessing the performance of 15 gothic like strakes. In addition, an assessment is needed regarding the variation of the maximum value of f for these same strakes with R_a. Furthermore, it may be useful to consider the rate at which f is increased for a given change in R_a for these strakes in order to gain an appreciation of the potential these shapes have to yield even higher values of f.

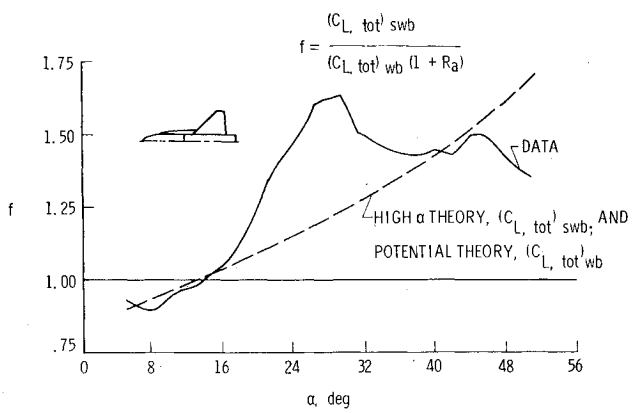

Fig. 13 Theoretical and experimental variation of f: AD 19; $M=0.2$.

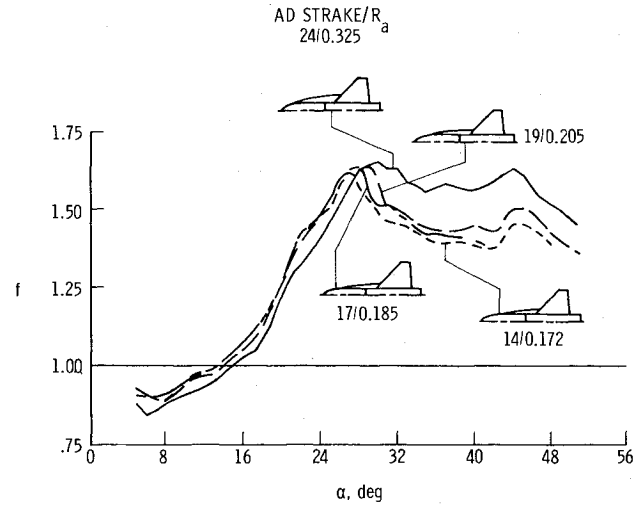

Fig. 14 Variation of f with α for most efficient strakes: $s_t>65$; $M=0.2$.

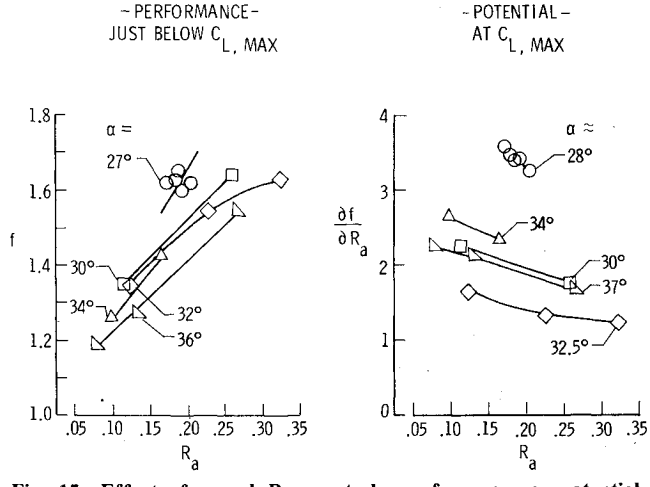

Fig. 15 Effect of α and R_a on strake performance or potential: gothiclike strakes; $M=0.2$.

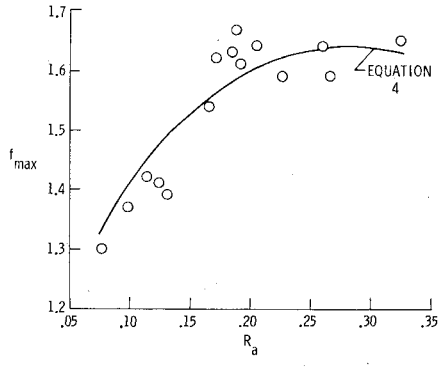

Fig. 16 Variation of f_{max} with R_a: gothiclike strakes; $M=0.2$.

Performance

Since f is dependent on α, as $C_{L,tot}$ is, as well as R_a, the f data are presented in Fig. 15 by groups. Each group of configurations has in common the fact that $C_{L,max}$ occurs at approximately the same value of α. In order to establish the f levels to be plotted on this figure, a particular or common value of α had to be chosen. The one selected for each group was determined from the criteria that 1) it be the smallest integer value for the group and that 2) it lead to $C_{L,tot}$ values for which strake-vortex breakdown had not commenced over the wing; i.e., $C_{L,tot} < C_{L,max}$. The figure shows that the groups are established for values of α of 27, 30, 32, 34, and 36 deg. Note that with the fairings used, all of which are roughly parallel, f increases with R_a for each value of α. Also, the results show that f decreases with α at a fixed value of R_a, and that it is possible to reach the same high level of f but with a smaller value of R_a and α. This latter R_a observation has previously been noted in the discussion centered on Fig. 14.

f_{max} Variation

The values of f plotted in Fig. 15 are not necessarily the maximum ones for each configuration. Those values, for f_{max}, are tabulated in Table 1 and graphed in Fig. 16. Through data analysis of these results, it was determined that f_{max} could be represented by the same function of R_a as was used for $\alpha_{BD\text{-}TE}$ in Eq. (1). In particular,

$$f_{max} = 1 + 0.64\sqrt{\sin[2\pi(R_a - 0.03)]} \tag{4}$$

Hence f_{max} and $\alpha_{BD\text{-}TE}$ are related by

$$f_{max} = 1 + 0.02\,\alpha_{BD\text{-}TE} \tag{5}$$

Figure 16 shows the data to be fairly well represented by Eq. (4).

Potential

One could assess the potential of these groups for producing larger f values upon being scaled up in R_a by examining the faired slopes of the f vs R_a data on the left side of Fig. 15. Though roughly parallel, they do differ in detail. In fact they show the $\alpha=27$ deg group to be highest with the $\alpha=34$ deg group next and the others lower. This is qualitatively the same results as graphed on the right side of Fig. 15 at $C_{L,max}$. The results for $\partial f/\partial R_a$ appearing on this figure were obtained by a different procedure. They were calculated from

$$\frac{\partial f}{\partial R_a} = \frac{1}{1+R_a}\left[\frac{1}{(C_{L,tot})_{wb}}\frac{\partial (C_{L,tot})_{swb}}{\partial R_a} - f\right] \tag{6}$$

with α fixed. This was done in Ref. 7 at the α required for $(C_{L,max})_{swb}$. There the $\partial(C_{L,tot})_{swb}/\partial R_a$ was determined by using data from the same group. The variation α within a group was ≈ 1 deg.

The importance of the $\partial f/\partial R_a$ results is that here is a group of strakes which yields a relatively high value of f_{max} and $C_{L,max}$ and do so at the correspondingly lowest angle of attack, while possessing the potential to form the genesis of other strakes which could obtain even higher values of f. These higher values, if obtained, would be expected to occur at $\alpha \gtrsim 30$ deg. Thus another criterion for measuring strake efficiency and performance, in terms of its potential, has been identified. It is this: to select the strake with the $\partial f/\partial R_a$ as large as possible, greater than 3, and the corresponding α associated with $C_{L,max}$ as small as possible.

Conclusions

A summary of an experimental and analytical study has been presented for 16 designed strake-wing configurations. These strakes have been designed from the hypothesis that the strake leading-edge suction distribution, especially its tip value, s_t, is important in establishing a strong strake-vortex system. Regarding this hypothesis, the following has been determined:

1) High values of s_t generally lead to higher values of the angle of attack at which the strake vortex begins to break down ahead of the wing trailing edge, $\alpha_{BD\text{-}TE}$. This was true in water and the correlation continues in air, though no formal correlation parameter has been established.

2) The largest values of the total configuration maximum lift coefficient, $C_{L,max}$, are generated for $s_t \geq 64$.

3) For $-70 < s_t < 100$, the more efficient strakes, in terms of lift generation per unit of exposed strake area, occur.

Other specific conclusions which are drawn from this wind-tunnel study at a Mach number of 0.2 follow:

1) High-angle-of-attack vortex lift theory reasonably estimates the lift up to strake-vortex breakdown.

2) High-angle-of-attack and low-angle-of-attack vortex lift theories bracket both the total and component pitching-moment data up to maximum lift or strake-vortex breakdown.

3) There are differences in $\alpha_{BD\text{-}TE}$ data obtained from the water and wind tunnels from 7 to 12 deg, with the air data being the larger. Though Reynolds number effects are present, the two sets of data do behave qualitatively the same.

4) $C_{L,max}$ increases with strake area, as expected, and has also been correlated to the strake span.

5) It is possible to generate essentially the same level of f, the additional lifting surface efficiency factor, with gothic strakes having areas from about one-half to two-thirds the size of the original gothic strake, which was designated the analytically designed (AD) 24 strake.

6) The maximum value of f can be simply related to $\alpha_{BD\text{-}TE}$.

7) Based on the strakes studied herein, those having $\partial f/\partial$ (strake area/reference wing area) >3.0 will belong to a family of strakes that are better performers and have the potential for being scaled up in area so as to yield new strakes that can obtain even higher values of f.

References

[1] Lamar, J.E. and Luckring, J.M., "Recent Theoretical Developments and Experimental Studies Pertinent to Vortex Flow Aerodynamics—With a View Towards Design (Review Paper)," AGARD CP-247 High Angle of Attack Aerodynamics, Jan. 1979.

[2] Smith, C.W., Ralston, J.N., and Mann, H.W., "Aerodynamic Characteristics of Forebody and Nose Strakes Based on F-16 Wind Tunnel Test Experience," NASA CR 3053, July 1979.

[3]Headley, J.W., "Analysis of Wind Tunnel Data Pertaining to High Angle-of-Attack Aerodynamics," AFFDL-TR-78-94, Vol. 1, July 1978.

[4]Lamar, J.E., "Analysis and Design of Strake-Wing Configurations," *Journal of Aircraft*, Vol. 17, Jan. 1980, pp. 20-27.

[5]Frink, N.T. and Lamar, J.E., "Water Tunnel Investigation of the Effect of Strake Design Variables on Strake Vortex-Breakdown Characteristics," NASA TP 1676, Aug. 1980.

[6]Frink, N.T. and Lamar, J.E., "An Analysis of Strake Vortex Breakdown Characteristics in Relation to Design Features," *Journal of Aircraft*, Vol. 18, April 1981, pp. 253-258.

[7]Lamar, J.E. and Frink, N.T., "Experimental and Analytical Study of the Longitudinal Aerodynamic Characteristics of Analytically and Empirically Designed Strake-Wing Configurations at Subcritical Speeds," NASA TP 1803, June 1981.

[8]Luckring, J.M., "Aerodynamics of Strake-Wing Interactions," *Journal of Aircraft*, Vol. 16, Nov. 1979, pp. 756-762.

[9]Lamar, J.E. and Gloss, B.B., "Subsonic Aerodynamic Characteristics of Interacting Lifting Surfaces With Separated Flow Around Sharp Edges Predicted by a Vortex-Lattice Method," NASA TN D-7921, Sept. 1975.

[10]Lambourne, N.C. and Bryer, D.W., "Some Measurements in the Vortex Flow Generated by a Sharp Leading Edge Having 65 Degrees Sweep," A.R.C. Tech. Rept., C.P. 477, 1960.